EXPERIMENTAL AND NUMERICAL ANALYSIS OF SUPERSONIC BLADE PROFILES DEVELOPED FOR HIGHLY LOADED IMPULSE TYPE STEAM TURBINE STAGES

R. Ghio - C. Raffaeli - A. Sabattini

Marine Systems and Components Business Unit, Fincantieri S.p.A., Genova, Italy
riccardo.ghio@fincantieri.it

V. Dossena - A. Fusetti - A. Spinelli - C. Osnaghi - F. Cozzi

Politecnico di Milano, Dipartimento di Energia, Via Lambruschini 4, 20157 Milano, Italy
vincenzo.dossena@polimi.it

ABSTRACT

The paper describes the results of a numerical and experimental research program addressing the aerodynamic investigation on the performance of blade profiles specifically developed for application in highly loaded impulse type turbine stages. The industrial requirements driving toward the adoption of highly loaded stage solutions are presented, along with an estimation of the profiles operating parameters. Two stator vanes and one rotor blade profile have been developed and extensively tested by means of flow field measurements and schlieren visualization in a transonic blow-down wind tunnel for linear cascades. Experimental results for the relevant operating conditions are presented, providing validation data for the CFD model used for blade design and evidencing that the main goals of the design optimization procedure have been achieved.

KEYWORDS

Supersonic Turbine, Shock Visualization, Supersonic Impulse Stage, Turbine Cascades

NOMENCLATURE

c	chord	h	blade height
s	pitch	o	passage throat
x	axial direction	b	axial chord
M	Mach number	Re	Reynolds number
N	number of blades	PS	pressure side
SS	suction side	U	turbine peripheral velocity
C	absolute flow velocity		

Greeks

ν	kinematic viscosity	α	flow angle
ζ	kinetic energy loss coefficient ($=\frac{V_{2,is}^2-V_2^2}{V_{2,is}^2}$)		

Subscripts and superscripts

2	cascade outlet	is	isentropic
T	turbulent	mix	mixed out

INTRODUCTION

In the market segment of small and medium steam turbine size for industrial, oil&gas and marine applications, requirements in terms of cost effectiveness and need for lightweight installations drive the development of compact machine solutions with increased load per stage. As a consequence of the high required stage load, for impulse type machines such as those manufactured by Fincantieri S.p.A., the stator blade channel will be operating in high expansion ratio conditions, resulting in transonic/supersonic flow regime in both nozzles and blades and close to tangential relative flow at rotor inlet. These aspects require the development of non-conventional aerodynamic profiles for both stationary and moving blades.

In the industrial steam turbine field, hardly any literature reference can be found dealing with the kind of optimization of concern to the present work, namely highly loaded impulse type turbine stages. A relevant work for industrial steam turbine applications was published by Rashid et al. (2007), mainly dealing with performance prediction variability of velocity compounded highly loaded Curtis stages, therefore focused on the supersonic aerodynamic interaction between nozzle and rotor. Conversely, other studies are available in the steam turbine literature where the methodological aspects and phenomena are similar to the present work, but the application deals with analysis and design of supersonic blade profiles used in last stages of large output steam turbines, see for instance the work of Váchová et al. (2015). Actually, the topic of increased stage loading driven by the advantages of lower stage count, and of the related blade profiles design and optimization, is often found in aerospace application, for example in the works of Wolf et al. (2010) and Sonoda et al. (2006), dealing however with reaction type stages optimization.

The challenging design goal is therefore to meet the market requirements as described above, ensuring a competitive level of efficiency for turbines with highly loaded impulse type stages. This can be obtained by means of achieving a blade profiles efficiency level in the supersonic design regime comparable to that attained with conventional blade design in subsonic range, still providing competitive performance in the off-design conditions. For this purpose, two new convergent-divergent nozzle profiles and a rotor blade profile have been specifically designed and optimized by means of two-dimensional CFD tools, and their performance tested and compared with experimental data taken at the Laboratorio di Fluidodinamica delle Macchine (LFM) of Politecnico di Milano.

AERODYNAMIC DESIGN PARAMETERS DEFINITION

In order to define the expected range of the design parameters for the blades airfoil, a representative application consisting of a steam turbine generator for waste heat recovery on a cruise ship has been considered. The steam turbine generator is part of a combined cycle with Diesel main engines and produces electrical energy through the recovery of excess steam not used by the ship services. Different waste heat recovery plant configurations were analyzed, based on thermal loads and steam consumption data supplied by the ship-owner. Having defined the steam turbine boundary conditions, a reference conventional design has been developed with the assumption that the stages operate at the optimal isentropic velocity ratio $U/C_0 \approx 0.48$ for impulse type stages. Specifically, the resulting machine consists of 6 stages with stator profiles operating in the high subsonic or transonic regime and with subsonic inlet relative velocity for rotor profiles, allowing the blading to be composed of profiles designed with conventional aerodynamic criteria. With the goal to deliver a lightweight and compact machine, as required by the application, different layout concepts with decreased number of stages were also analyzed with the effort to achieve the low cost target. It was found that decreasing the number of stages up to 4 rather than the 6 of the conventionally loaded reference solution resulted in rotor inlet relative Mach number approaching 1.0 and in nozzle exit Mach number peaking at maximum values of 1.5 for the two intermediate stages. Moreover, the rotor inlet relative flow angle was reduced to approximately 20°, while the inter-stage absolute flow angle increased to 127° (see top left of Figure 1 for angle reference direction). All these aspects are

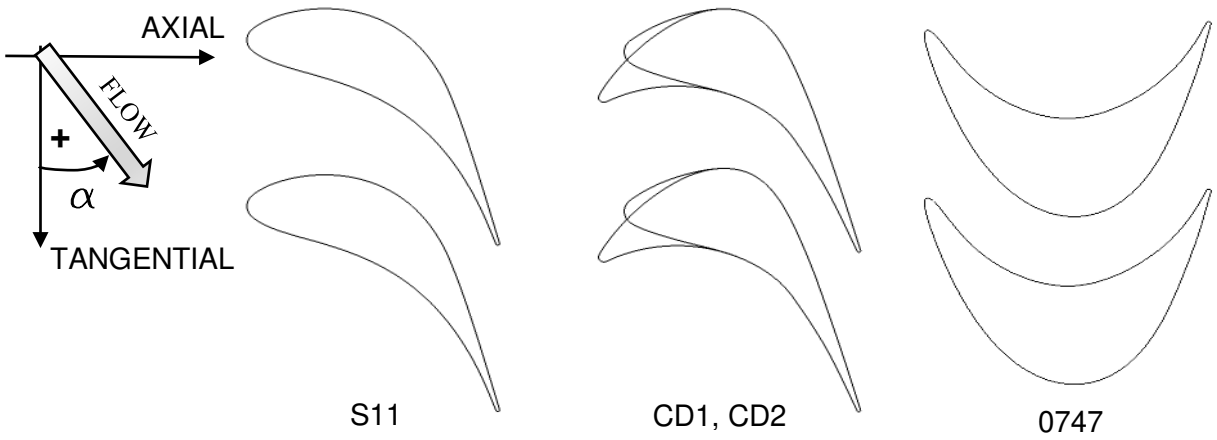

Figure 1: Channel geometry: conventional transonic nozzle S11; convergent-divergent supersonic nozzles CD1 and CD2; rotor impulse profile 0747.

consequences of the increased stages load, as indicated by the isentropic velocity ratio being reduced to approx. U/C_0=0.28.

The blade design effort was subsequently undertaken, with different design philosophies adopted for the stationary and for the moving blades sections. Two stationary blade sections were designed for the same expected outlet Mach number range: the CD1 profile was designed for a purely axial inlet flow, typical of the turbine first nozzle, while the CD2 profile was designed for a nominal inlet angle of 130° typical of an intermediate high loaded turbine stage. The design Mach number for the nozzles was set in the range 1.2-1.4, slightly lower than the maximum expected Mach regime for the described application, choosing a proper exit to throat area ratio; this ensures avoiding high losses in nozzle profiles at off-design operation. Particular care has been devoted to the design of the rear portion of the nozzle in order to avoid discontinuous curvature in the supersonic part of the nozzle geometry. In the present paper, the measured performances of the new geometries are presented and compared to those of the reference transonic profile (S11), commonly adopted for applications with conventional $U/C_0 \approx 0.48$. The impulse type moving blade profile design mainly addressed the leading edge portion, where high flow velocities arise due to acceleration on the suction side, and where, in case of rotor inlet relative Mach number approaching 1.0, a pocket of supersonic flow and associated shocks occur, causing a reduction of conventional profile performance. The blade profile was therefore modified in such a way to minimize the strength of the suction side shock in order to make it more tolerant to low values of inlet flow angle by means of a reduction in suction side curvature and inlet metal angle. The resulting moving blade geometry (0747) allows reducing losses compared to conventional design profiles in the high subsonic/transonic operating range.

Sketches of the conventional profile S11 together with the two convergent divergent nozzles (CD1 and CD2) and the new rotor profile (0747) are reported in Figure 1, along with the reference direction used for absolute and relative flow angle definition.

EXPERIMENTAL SETUP AND TEST MATRIX

The measurements campaign was carried out in the transonic wind tunnel for linear cascades of the Laboratorio di Fluidodinamica delle Macchine at the Politecnico di Milano. This is a blow–down facility fed by 6000 kg of pressurized stocked air. The maximum sizes of the test section are 80 mm height and 470 mm width. The stator cascades were composed by 8 blades, using a scale factor of 2:1 compared with the original size of the profiles. For the rotor analysis, a scale factor of 2:1 resulting in an aspect ratio of 2 was used in order to avoid the presence of secondary flows in the measurement zone at mid span, due to the large deflection imposed (≈140°) to the flow. Consequently, the rotor cascade was composed of 12 blades.

A movable tailboard placed downstream of the cascade ensures the periodicity condition.

The flow field downstream of the cascade was tangentially traversed by a miniaturized 5 hole probe (head of 1.8 mm) pre-aligned with the expected average flow angle at a distance of 33% of the blade axial chord. The 5 hole probe was calibrated in a reference Mach number ranging from 0.3 to 2.35, on a yaw and pitch angle range of ±20°. For the supersonic cases, a total pressure correction corresponding to that of the normal shock at the relevant Mach has been considered during calibration.

The 5 hole probe uncertainty associated to the local value of ζ is $0.25 \cdot 10^{-2}$, while ±0.25° is the uncertainty in the flow angle measurement. The data reported above, based on a confidence level of 95%, are not valid when the probe head is crossed by a shock. Under this condition, the pressure gradient evaluated on the probe head diameter may become dramatically high, and the results obtained by the calibration performed under uniform flow conditions are not representative any more. Therefore, the pressure difference across the probe head is interpreted as a high yaw angle and, consequently, a relevant error in the local flow angle and static pressure may be introduced. This effect is clearly visible in the traversing results performed at high Mach number (Figures 6 and 10), where the measurement points neighbouring the shock show relevant discontinuities in flow angle and Mach number distributions. It should be underlined that this is only a local effect, partly influencing the pitchwise averaged data. More details about the experimental facility and the measurement technique can be found in Dossena et al. (1996, 1999) and D'Ippolito et al.(2011).

The measurement grid downstream of the three stator cascades was defined by 71 points equally spaced by 1.5 mm; 53 points spaced by 1 mm defined the measurement grid adopted for the rotor cascade. In all the cases and for every expansion ratio, a minimum of two blade passages was covered in order to verify the establishment of a proper periodicity condition as resulting from the position of the downstream tailboard. The reference upstream flow was provided by a three hole probe, positioned approximately one axial chord from the profile leading edge. A flow turbulence intensity lower than 1% was measured at the cascade inlet by means of hot wire anemometry.

With reference to the three stator profiles, a wide range of expansion ratios (M_{2is}=0.6 - 1.7) was analyzed by means of approximately 10-15 tests for every considered incidence angle. For the rotor cascade, the range of M_{2is}=0.6-1.1 was explored by approximately 8 tests for every incidence angle.

A summary of the experimental test grid, together with the main characteristics of the four cascades, are reported in Table 1. A total number of approximately 40 pressure taps machined on the pressure side and suction side of two adjacent blades allowed to obtain the distribution of isentropic Mach number on the mid span section of the blade channel. 25 pressure taps, located on the endwall plate in correspondence to the traversing section, give the reference static pressure for the tests.

Cascade designation	Nominal inlet flow angle (α)	Incidence angle	M_{2is}	$Re \cdot 10^6$	h/c	s/c	c	N
S11	90°	0	10-15 tests in the range 0.6 -1.7	1.2-4.2	0.86	0.54	93.3	8
CD1	90°	0, +30°, +50°		1.2-5.2	0.86	0.54	93.1	8
CD2	130°	-20°, 0, +10°		1.5-5.6	0.90	0.57	89.2	8
0747	20°	0, +1°, +2°	8 tests in the range 0.6 - 1.1	0.7-1.5	2	0.66	40.0	12

Table 1: Summary of aerodynamic tests performed in the LFM blow-down wind tunnel and main cascades characteristics.

A double passage schlieren system has been adopted to visualize shocks in the test section. In this configuration, the emitting and the receiving optical components lie on the same optical bench, allowing an easy alignment with respect to a conventional Z-type set-up. The light emitted by a 1.12 W blue LED is focused and then collimated by a spherical mirror (150 mm diameter). The collimated light rays traverse the test section twice: the light beam is reflected back to the same spherical mirror by the mirror-polished cascade endwall. The knife orientation is such that positive density gradients (compression waves and shocks) appear as darker regions, while expansion waves appear brighter.

NUMERICAL SETUP

The computations were carried out by means of the commercial suite of codes FINE/Turbo v9.1-2, both for the blade profiles development activity and for the numerical analyses performed with the purpose to compare CFD results with detailed experimental data.

The design phase computations were run with default setup parameters suggested by the codes, resulting in stable computations with good convergence behavior, which allowed for fast development work. However, when the details of the flow field were analyzed for comparison with test data, it was found that this choice produced results characterized by some inconsistency, such as local negative levels of loss and excessive diffusion for wake prediction. This kind of results was also reported in Wolf et al. (2010), where the same code was applied to simulate a very similar operating condition. Therefore, in order to improve the physical consistency of the numerical results, CFD data have been obtained with an improved numerical setup, resulting from a sensitivity analysis to grid size and shape. The final grid differs from the default one for the increased number of grid points and for the alignment with the wake direction. Furthermore, a second order upwind spatial discretization scheme was selected. It was found that the mentioned changes proficiently improved the detailed flow field prediction when compared to test data, even if showing higher levels of global residual (the difference to the default set up is approximately 3 orders of magnitude, depending on the case), because the computations were less stable due to the selected numerical scheme. Nevertheless, the mass flow rate error is negligible in all cases (relative mass flow error lower than 0.025%), indicating that the overall solution is actually stable and that the high residual values represent some localized small instability in the flow field.

All the profiles were studied in a 2D planar cascade configuration, with two blade-to-blade mesh layers in spanwise direction, where a symmetry condition was applied to enforce two dimensional flow. The multi-block mesh topology was provided for all cases by the Autogrid5 default O4H template with upstream and downstream blocks, with an angle control for wake alignment applied for the stator blade profiles. As an example, Figure 2 shows the multi-block computational domain and the grid topology adopted for the S11 reference nozzle computations. The main overall grid quality parameters are reported in Table 2.

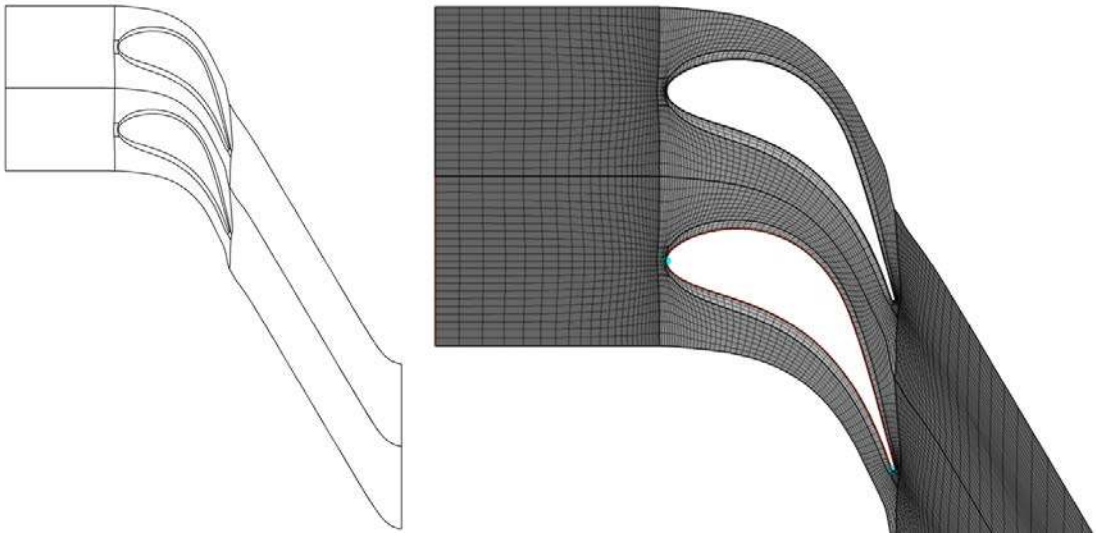

Figure 2: Multi-block computational domain with downstream wake alignment: O-grid block around the profile; 4 H-grid blocks surrounding the O-grid; upstream and downstream H-grid blocks.

	S11	CD1	CD2	0747
Points number per layer	72707	68335	68735	46291
Minimum skewness angle	18°	19°	16.8°	54°
Maximum expansion ratio	2.6	2	1.5	1.3

Table 2: Main computational grid parameters for the four cases.

Steady state fully turbulent RANS were solved with the provided second order upwind discretization scheme, using the Spalart-Allmaras model for turbulence modeling and air assumed to be a perfect gas as working fluid. Given the different blade sections' geometries and the wide range of operating pressure ratio, the y+ parameter shows different values depending on the case, but the average y+ value of points closest to the blade surface is always lower than 10 for all presented cases.
The inlet boundary conditions were prescribed by constant total pressure, total temperature and inlet flow angle, while an average value of static pressure is applied at the outlet region. The turbulent viscosity imposed at inlet corresponds to a turbulent to molecular viscosity ratio $\nu_T/\nu = 2$. Inlet and outlet boundary regions were located approximately 1 axial chord upstream and 1.5 axial chord downstream of the blade for all the analyzed blade geometries.

ANALYSIS OF RESULTS

Experimental tests have been initially carried out on a purely convergent transonic stator profile (S11). This first experimental data set has been used for the definition and the validation of the best computational setup and numerical scheme. Then, the same numerical approach has been applied to the subsequent analyses of the two new convergent-divergent stator profiles (CD1 and CD2) and of the rotor profile (0747). Further on, experimental tests have been performed on both convergent-divergent vanes and on the rotor blade. The broad test matrix, including a wide range of expansion ratios and incidence angles for every considered profile, has been summarized in Table 1, where the main cascades geometrical parameters are also reported.
The pitchwise distribution of the local kinetic energy loss coefficient (ζ) and outlet flow angle (α_2) at a distance equal to 33% of the axial chord from the trailing edge support the analysis and the comparison of numerical to experimental data; the surface isentropic Mach number distributions will also be presented for the same purpose. Furthermore, only for transonic and supersonic outlet conditions, schlieren pictures and contours of the projected density gradient magnitude are also proposed, compared and discussed. To ensure proper resolution of density gradients, the projection direction was set to the estimated streamwise direction -given by the arcsin(o/s)- for the nozzles, and to the tangential direction for the rotor blade.

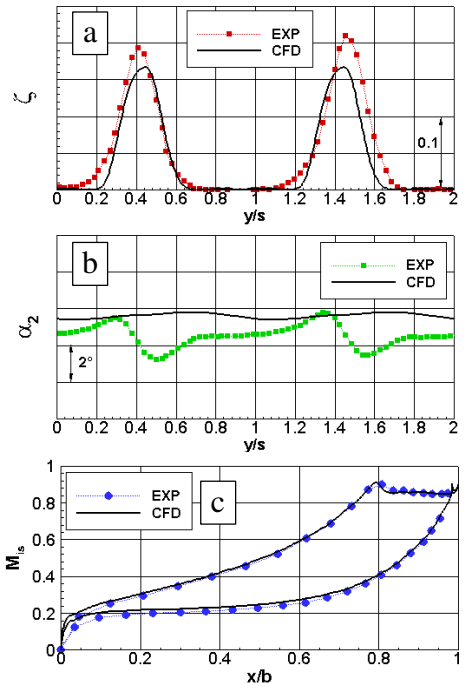

Figure 3: S11 at $M_{2,is}$=0.83: pitchwise distribution of ζ (a) and flow angle (b) at x/b= 0.33. Isentropic Mach number distribution on blade surfaces (c).

For the sake of brevity, only results of some selected cases (subsonic, transonic and supersonic) concerning the nominal incidence for S11 and CD2 vanes will be here presented, followed by two representative cases for the 0747 rotor profile at the most severe incidence condition.

S11: convergent transonic stator profile (reference)

The experimental and numerical results obtained at three outlet isentropic Mach numbers (i.e., M_{2is}=0.83, 1.19, 1.67) in the representative range for the stage load, are presented and discussed below.
The results at M_{2is}=0.83 are presented in the three frames of Figure 3, where frame (c) evidences an excellent agreement between the experimental and the numerical isentropic Mach number distribution all along the blade surface. As evidenced by frame (a), the final numerical CFD set up, based on an upwind scheme, correctly predicts the presence of the isentropic plateau outside of the wake, but slightly underestimates the kinetic energy loss peaks associated with the maximum velocity defect in the wake. This difference can be ascribed to an excessive diffusion operated by the CFD code.

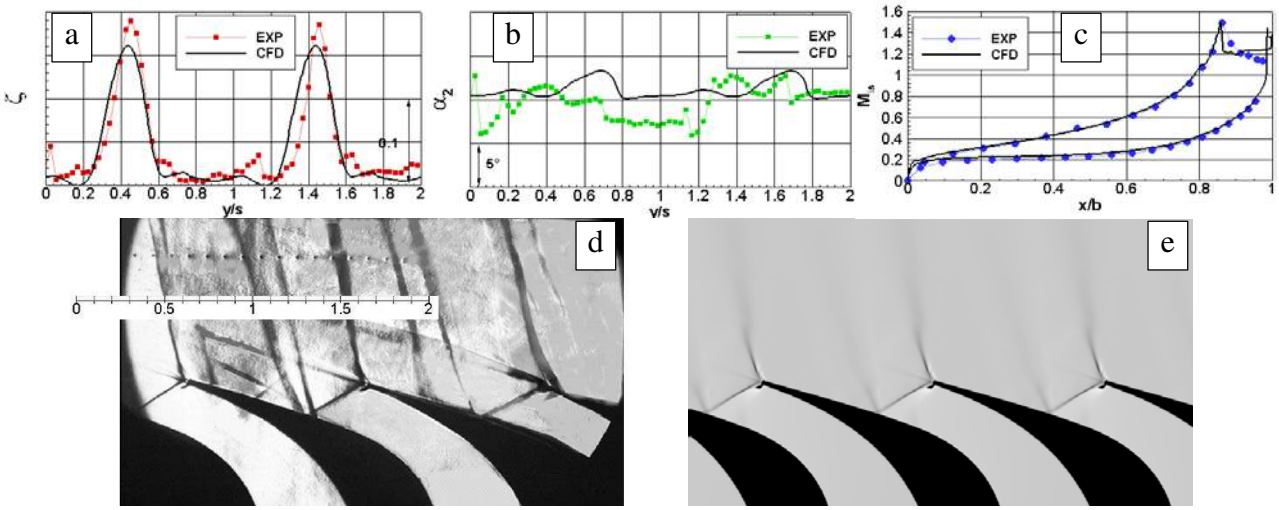

Figure 4: S11 at $M_{2,is}$=1.19: pitchwise distribution of ζ (a) and flow angle (b) at x/b= 0.33; Isentropic Mach number on blade surfaces (c); schlieren picture (d) and magnitude of the streamwise density gradient from CFD data (e).

Moreover, the profile kinetic energy loss obtained by CFD, evaluated both by a pitchwise mass averaged or by a mixed out procedure, only slightly differs from that evaluated by the experiments as it will be shown in the following. Figure 3 frame (b) shows that CFD underestimates the averaged flow deflection by approximately one degree, while the experimental distribution evidences a higher flow angle variation along the pitch, confirming the already mentioned excessive numerical diffusion.

The comparison of results for the low supersonic case M_{2is}=1.19 is presented in Figure 4, where the schlieren picture and the streamwise projected density gradient contours derived by the CFD data are reported in frame (d) and (e).

From the comparison between the experimental and "numerical" schlieren pictures (frame (d) and (e)) it is possible to infer that the main shock structure is well predicted by the computation as witnessed by the very well captured direction and position of the two shocks starting from the trailing edge. Conversely, the numerical flow model does not correctly predict the complex phenomenon associated to the impingement of the shock on the SS boundary layer, remarkable in the schlieren picture. A closer look at the interaction region for the same case of Figure 4 frame (d) is reported in Figure 5. The incoming shock "a" and the two generated shocks "b" and "d" can be easily identified. The very small white region close to the wall (label "c"), where the negative spatial density gradient increases, can be identified with an expansion fan. Unfortunately, the outer region of the fan cannot be identified due to the very low value of the density gradient.

The mechanism evidenced by the schlieren picture can be consistent with the interaction of the shock with a laminar boundary layer, as described by Shapiro (1953) and reported in Figure 5 (left frame). As the shock "a" enters the boundary layer, it weakens due to the progressive Mach number reduction approaching the wall. Finally, the shock vanishes in the inner subsonic boundary layer.

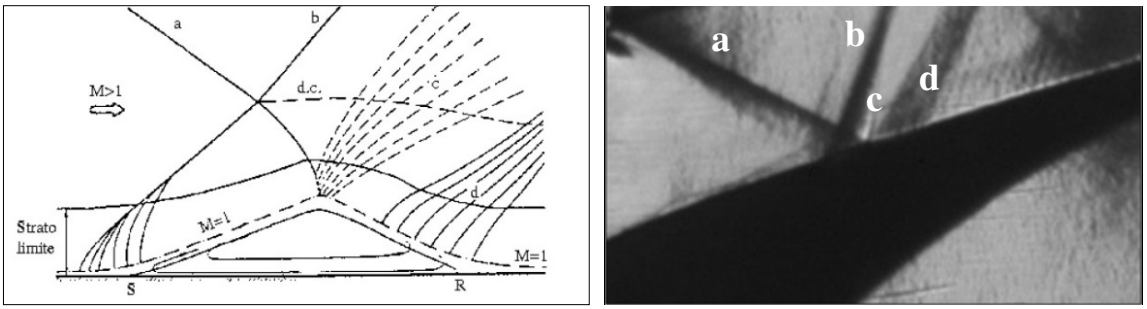

Figure 5: Interaction of a shock wave with a laminar boundary layer. Left: sketch taken from Shapiro (1953); right: local zoom from Figure 4 (frame (d)).

The pressure increase generated downstream of the shock propagates upstream through the subsonic boundary layer near the wall, generating a separation zone caused by the steep adverse pressure gradient. This separation bubble forces the supersonic incoming flow to deflect counterclockwise through a series of compression waves that merge to form a new shock wave "b". Afterward, the flow follows the profile of the separated region turning clockwise through an expansion fan "c". Before returning to follow the wall, the flow must experience another counterclockwise rotation, obtained through a series of compression waves "d" that finally merge into another shock wave further downstream. Once the flow has passed the separation bubble, it returns to follow the blade profile regularly. In conclusion, the interaction of shock "a" produces two shocks "b" and "d" and an expansion fan "c". The presence of a laminar boundary layer on the rear part of a supersonic turbine nozzle can be considered as surprising but it is not a novelty. Váchová et al. (2015) evidenced a similar difference between flow visualizations and numerical computations, while testing the application of a Transition Model on a supersonic turbine at an outlet Re of about $1.5 \cdot 10^6$ and for an outlet isentropic Mach similar to the case reported in Figure 5. They showed that the presence of a single reflected shock wave in the CFD results (as also reported in Figure 4 frame (e)) can be related to the setting of a fully turbulent computation (as in the present case). Conversely, when a laminar computation or a proper transition model is considered, a second reflected shock appears downstream, in accordance with the schlieren visualization reported in the present paper as well as in Váchová et al. (2015) and with the scheme presented in the left frame of Figure 5. Moreover, in the same region, the isentropic Mach number distribution (Figure 4, frame (c)) presents slightly different values between experimental and numerical results where the shock impacts on the profile SS. The numerical kinetic energy loss traverse evidences in the wake region peak values slightly underestimated compared to the experimental ones. Furthermore, the experimental loss distribution shows fluctuations along the pitch, clearly associated with the shock reflections coming from the tailboard and from the neighbouring suction side. The same feature can also be found in the experimental pitchwise distribution of α_2, showing high discontinuities along the blade pitch. It is evident that the downstream tailboard introduces, for the particular case, disturbances and modification in the flow field, with respect to the actual application. This limit in linear cascade testing at supersonic Mach number is well known and can hardly be avoided, as also reported by Wolf et al. (2010). Moreover, since the location of the shock reflected by the tailboard is a function of both the Mach number and the position of the tailboard, the test condition mostly affected by this spurious effect cannot be easily foreseen.

The representative quantities obtained for the high supersonic case at M_{2is} =1.67 are presented in Figure 6.

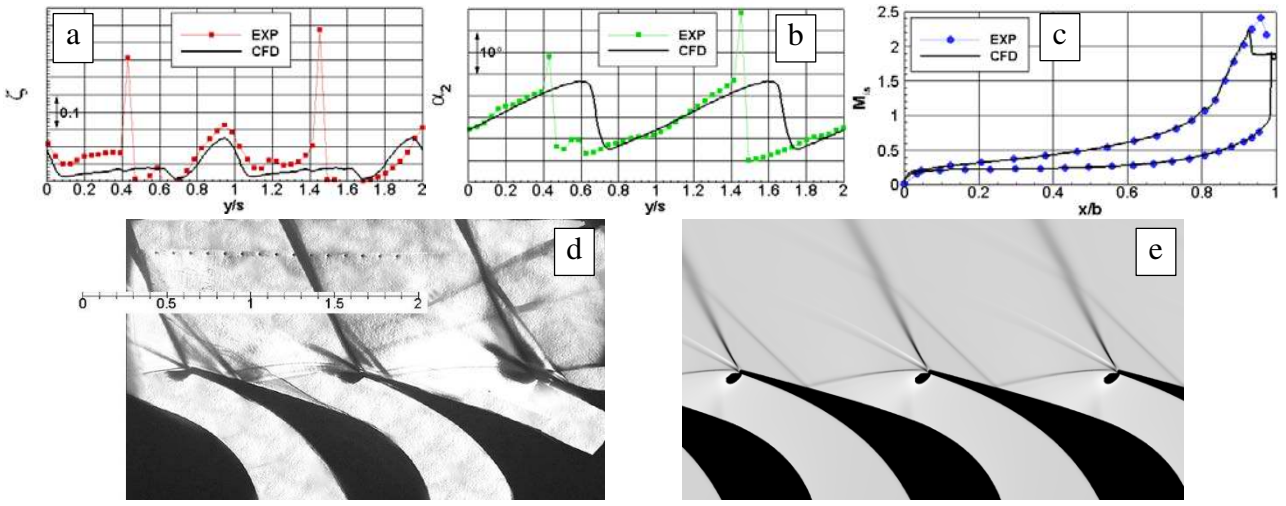

Figure 6: S11 at $M_{2,is}$=1.67: pitchwise distribution of ζ (a) and flow angle (b) at x/b= 33%; Isentropic Mach number distribution on blade surfaces (c); schlieren picture (d) and magnitude of the streamwise density gradient from CFD data (e).

The comparison between the Mach number distributions in frame (c) shows that the impact of the shock on aft part of the blade SS is slightly advanced by the numerical results. This difference is also reported in the two images presented in frame (d) and (e), where some differences in the shock structures can be identified: the position of the shock impact on the SS is advanced and, as a consequence, the reflected shock also shows a different inclination. It is interesting to notice that the schlieren picture also evidences that the shock structure is not perfectly periodic because of the presence of the reflected shock coming from the tailboard, influencing the development of the SS boundary layer. The blade positioned on the right side of frame (d) shows a better agreement of the shock structure with the numerical solution: this condition may be related to the absence of the spurious effect produced by reflection on the tailboard, hardly recognizable in this passage. Nevertheless, both ζ and α_2 distribution evidence a quite perfect periodicity condition. The kinetic energy loss distribution (frame (a)) confirms a good agreement of the loss level associated with the wakes and a slightly higher experimental value in the central part of the channel outside of the wake. Moreover, the overshooting shown in the experimental data exactly corresponds to the strong shock detaching from the SS of the trailing edge. As previously discussed, the passage of the probe head through the strong shock leads also to an overestimation of the flow angle, displayed in frame (b) by a similar overshoot positioned exactly at the same tangential location. Figure 7 presents and compares the experimental and numerical profile losses vs. the mixed out isentropic Mach number, in terms of kinetic energy loss coefficient computed starting from the flow mixed out quantities. Starting from the subsonic range up to low supersonic regime a good agreement between experimental and numerical profile losses can be observed. In the high supersonic regime the experimental values are always higher than the numerical ones. Even if the effects produced by the shocks reflected from the tailboard may generally lead to an overestimation of losses - as also reported by Wolf et al. (2010) -, it should be remarked that the local loss values associated with the trailing edge shock system in CFD results are, in general, very low, contributing to the remarkable difference observed at the higher expansion ratios.

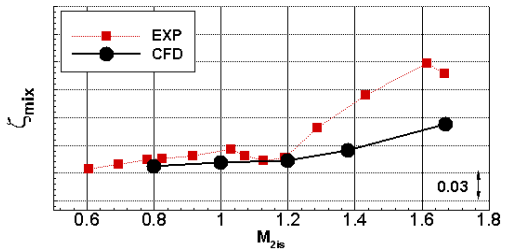

Figure 7: Experimental and numerical mixed out kinetic energy loss for the S11 profile.

CD2: convergent-divergent supersonic stator profile

Three cases ranging from transonic to supersonic regime are presented for the convergent-divergent profile. Figure 8 shows the results obtained for M_{2is}=1.03.

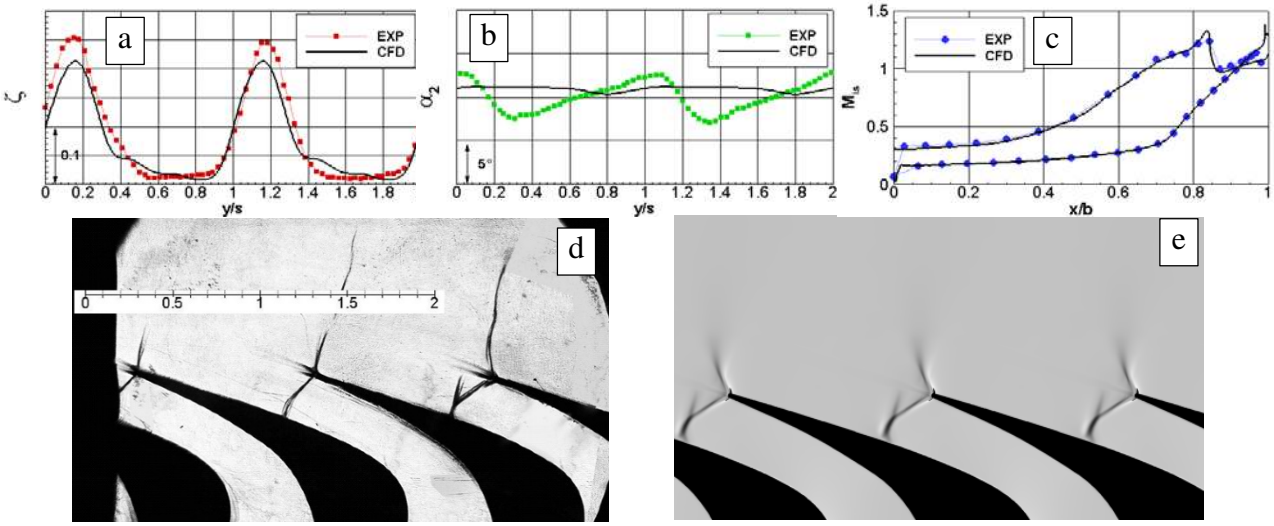

Figure 8: CD2 at $M_{2,is}$=1.03: pitchwise distribution of ζ (a) and flow angle (b) at x/b= 33%; Isentropic Mach number distribution on blade surfaces (c); schlieren picture (d) and magnitude of the streamwise density gradient from CFD data (e).

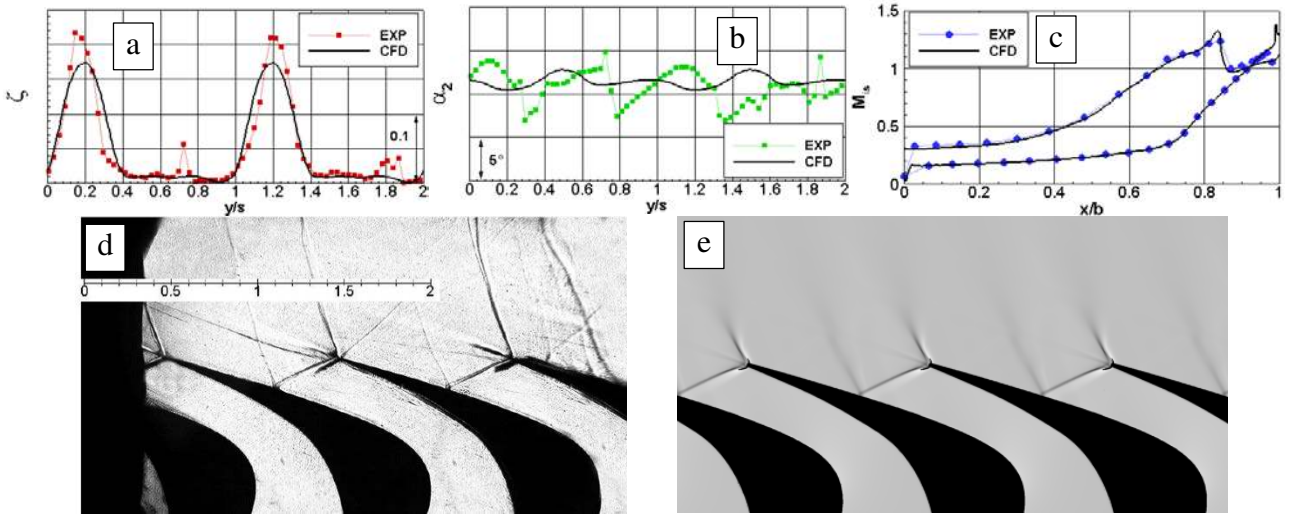

Figure 9: CD2 at $M_{2,is}$=1.26: pitchwise distribution of ζ (a) and flow angle (b) at x/b= 33%; Isentropic Mach number distribution on blade surfaces (c); schlieren picture (d) and magnitude of the streamwise density gradient from CFD data (e).

Although this transonic condition was quite unstable during the tests, the experimental isentropic Mach number distribution along the blade profile (frame (c)) is in good agreement with the numerical solution: the extent and the location of the normal shock occurring at the exit of the blade channel is well predicted as also confirmed by the schlieren pictures. With reference to Figure 8 frame (a), the zone located between two adjacent wakes evidences a non-zero loss plateau related to the normal shock that develops in the rear part of the bladed channels. The peak losses only reveal a small difference between CFD and experiments. The angle distribution in frame (b) shows a fairly good agreement in the averaged value, but, as in the previous cases, the CFD distribution is dramatically smoother than the experimental reference, with peak differences up to 4°.

The low supersonic case corresponding to M_{2is}=1.26 is summarized by the 5 frames in Figure 9, presenting flow features very similar to those discussed above.

The intensity and the position of the oblique shock starting from the trailing edge are well predicted as can be observed from the two schlieren images in frames (d) and (e). The low loss peaks appearing between the wakes are associated to the shock starting from the trailing edge and impacting on the SS of the adjacent blade. Although in the image that represents the density gradient magnitude the trace of the reflection appears, the numerical prediction of the associated loss on the measuring traverse is negligible, as already evidenced in other similar cases.

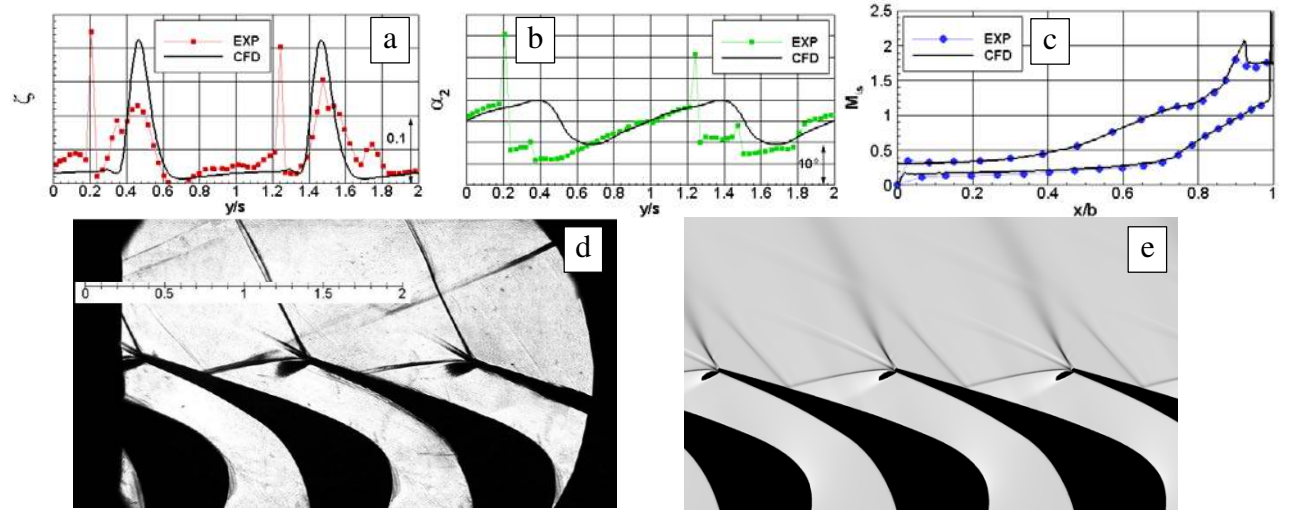

Figure 10: CD2 at $M_{2,is}$=1.614: pitchwise distribution of ζ (a) and flow angle (b) at x/b= 0.33; Isentropic Mach number on blade surfaces (c); schlieren picture (d) and magnitude of the streamwise density gradient from CFD data (e).

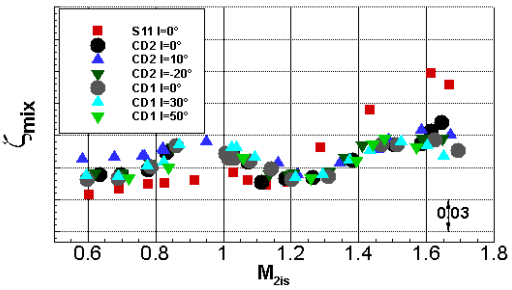

Figure 12: Experimental mixed out kinetic energy loss for the three stators as a function of the outlet isentropic Mach number in the considered range of incidence angles.

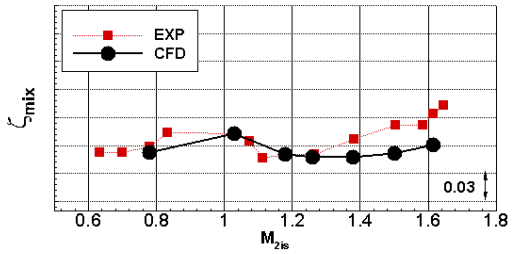

Figure 11: Experimental and numerical mixed out kinetic energy loss for the CD2 profile.

Figure 10 reports the results obtained at the highest supersonic test, corresponding to M_{2is} = 1.61.

The numerical isentropic Mach number distribution along the blade is again in good accordance with the experimental one, except for the impact zone of the shock on the suction side; it is also possible to suppose that only the M_{is} peak value is lost in the experiment, due to the very steep gradient and to the pressure tap discretization. It is remarkable that the pressure trend upstream of the shock matches perfectly. The experimental kinetic energy loss traverse presents three regions of loss along the blade pitch: the higher peak can be related to the trace of the strong SS shock starting from the blade trailing edge, remarkable in the schlieren picture, while a second one is associated with the wake. The third and lower peak is associated with the shock reflected by the blade SS. The same shock system is not so evident in the CFD results of frame (a), both due to the lower loss level always associated to the shocks and to a small difference in the shock angle. As a result, the main shock leaving the blade trailing edge and the one reflected by the blade SS, merge with the wake almost in the same axial position of the traverse reported in frame (a). Therefore, only for this case, the peak values of losses associated to the wake are higher in CFD results than in the measurements.

Figure 11 shows the comparison between experimental and numerical mixed out values of kinetic energy loss as a function of the mixed out isentropic Mach number. As already observed for the S11 profile, a very good agreement can be found between experimental and numerical values from the subsonic to the low supersonic regime whilst a significant divergence emerges in the supersonic regime, only partly justified by the presence of the tailboard reflected shocks that, for the particular cases, did not play a relevant role.

Figure 12 summarizes the experimental results related to the three nozzles, in terms of ζ_{mix} for all considered incidence angles and Mach numbers. The plot displays that both the convergent – divergent nozzles are quite insensitive to the considered incidence variation. At the same time a significant loss reduction in the range 2–5% is achieved for a Mach number higher than 1.2.

0747: rotor profile

In order to verify the sensitivity to incidence conditions of the newly designed impulse profile in the high subsonic/transonic regime, experimental tests and CFD calculations at inlet flow angles lower than nominal have been also performed. The mixed out kinetic energy loss for the most severe inlet flow angle (approximately 18°, corresponding to 2° of positive incidence) in the considered Mach number range is shown in Figure 13. A general good agreement in the design operating range (M_{2is}>0.9) can be observed in the plot, while the data present an increasing difference reducing the Mach number below the design range. Experimental and numerical flow field details for the nominal outlet Mach number (M_{2is}=1.03) are shown in Figure 14. The numerical analysis well captures the presence of the shock at the blade leading edge, as remarked in the projected density gradient representation. Moreover, the experimental isentropic Mach number profile also identifies the same peak

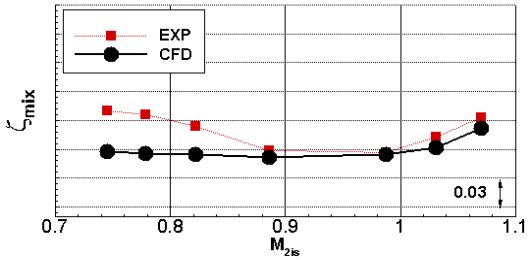

Figure 13: Experimental and numerical mixed out kinetic energy loss for 0747 rotor profile.

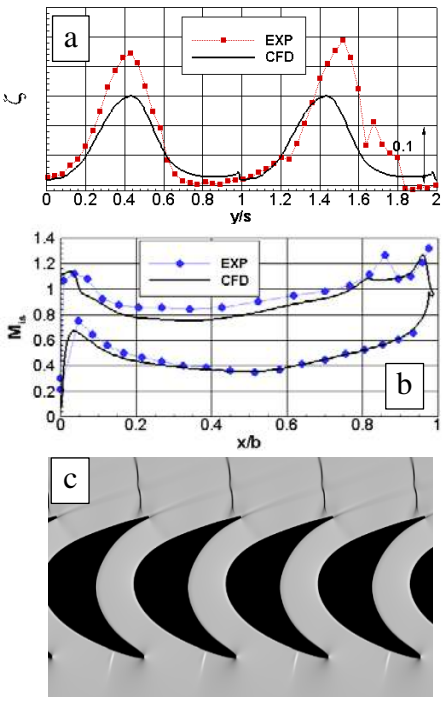

Figure 14: Rotor profile 0747 at $M_{2,is}$=1.03: pitchwise distribution of ζ at x/b= 0.33 (a); Isentropic Mach number on blade surfaces (b); magnitude of the tangential density gradient from CFD data (c).

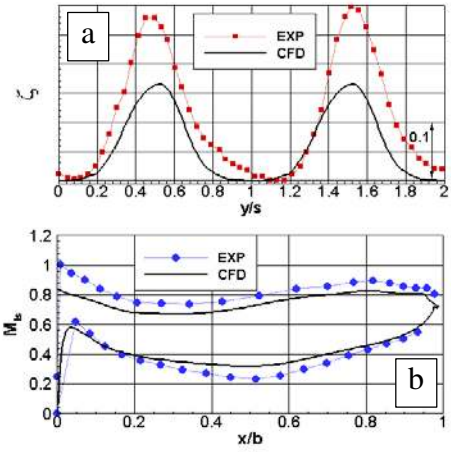

Figure 15: Rotor profile 0747 at $M_{2,is}$=0.75: pitchwise distribution of ζ at x/b= 0.33 (a) and Isentropic Mach number on blade surfaces (b).

velocity in the initial part of the suction side, but shows higher values along the suction side of the channel and highlights the presence of a second shock impacting the rear part of the suction side which is not detected by the numerical results. The loss traverse indicates a good agreement in terms of wake width prediction, but the peak loss values associated with the wake appear to be underestimated by the computation, most likely due to the misalignment between the grid and the wake direction.

Focusing now on the subsonic case corresponding to M_{2is}= 0.75 (Figure 15), the kinetic energy loss traverse presents differences of the same order of the nominal case in the center of the wake. On the contrary, the width of the wake is dramatically underestimated by CFD evidencing an isentropic flow region extending for ¼ of the pitch, while only one measuring point shows a zero value along the pitch. Consistently, the surface isentropic Mach number distribution measured on the profile SS, displays a significant higher deceleration on the front part, probably not accurately predicted by the computation, based on a more stable fully turbulent modeling. A similar trend, characterized by a smaller difference, can be noticed on the center part of PS distribution. Both mentioned diffusions suggest a more intense thickening of the boundary layer in the blade channel, leading to the remarkable difference experienced in the profile loss value evidenced in Figure 15 frame (a).

CONCLUSIONS

Experimental tests were carried out on two supersonic nozzle profiles and on a moving blade profile developed for application in highly loaded impulse stages. Tests were also performed on a reference transonic nozzle of conventional design. Test data were compared over a wide range of operating conditions against the results of computations performed with a commercial CFD code.

Only selected relevant cases are shown in the paper.

For subsonic and transonic conditions a good agreement was generally achieved between CFD and tests. The detailed flow field comparison allowed also to improve the physical consistency of the computational results by means of a convenient selection of the main numerical setup parameters.

Only for some cases at the highest supersonic regime, some differences between experimental and numerical results were found, highlighting some difficulties in resolving the flow features with both approaches. Nevertheless, a detailed analysis of most relevant cases, also supported by schlieren images, allowed to attribute the mentioned discrepancies mainly to code diffusivity and to the effects produced by high gradients on the measurement probe. In some particular cases, shock reflections from the solid tailboard produced spurious effects on the downstream flow field.

Moreover, the test results confirmed that the goals of the profile design procedure were satisfactorily achieved: the performance of the two nozzles in the expected operating range (M_{2is}>1.2) turned out to be considerably higher than the reference transonic nozzle. At the same

time, the loss increase in the subsonic range is limited, allowing the profile to be safely used also in off-design far from the conditions considered in the design process, which mostly addressed supersonic expansion ratios.
For the moving blade the minimum loss operation is indeed found to occur in the expected Mach number range for all the considered incidence angles. Despite the numerical and experimental mixed out losses show comparable values in the design high Mach number regime, the detailed flow field comparison highlights areas where significant differences occur, most likely due to both numerical and physical effects, and further research activity would be needed to improve the flow field understanding and identify the sources of the above mentioned differences.

ACKNOWLEDGEMENTS
The work presented in this paper was carried out within the framework of the Italian research project FluMarTurb DM62588 funded by MIUR (Ministry of University and Research) and DLTM (Distretto Ligure delle Tecnologie Marine), whose support is gratefully acknowledged.

REFERENCES
Shapiro A.H (1953) "The Dynamics and Thermodynamics of Compressible Fluid Flow", John Wiley & Sons Inc.
Dossena V**.**, Osnaghi C. et al., *"On Testing The Aerodynamics Of Film-Cooled Blades"*, (1996). Proceedings of the XIIIth Symposium on measuring techniques on transonic and supersonic flows in cascades and turbomachines, Zurich
Dossena, V., Perdichizzi, A., and Savini, M., (1999), *"The Influence of Endwall Contouring on the Performance of a Turbine Nozzle Guide Vane"* ASME J. Turbomach., 121(2), pp. 200–208
D'Ippolito, G., Dossena, V., and Mora, A., (2011), *"The Influence of Blade Lean on Straight and Annular Turbine Cascade Flow Field,"* ASME J. Turbomach., 133(1), p. 011013
Sonoda, T., Arima, T., Olhofer, M., Sendhoff, B., Kost, F., Giess, P.-A., (2006). *A Study of Advanced High-Loaded Transonic Turbine Airfoils*. Trans. of the ASME, Vol. 128, October 2006
Rashid, S., Tremmel, M., Waggot, J., Moll, R., (2007). *Curtis Stage Nozzle/Rotor Aerodynamic Interaction and the Effect on Stage Performance*. Journal of Turbomachinery, Vol. 129, July 2007
Wolf, T., Kost, F., Janke, E., Haselbach, F., Willer, L., (2010). *Experimental and Numerical Studies on Highly Loaded Supersonic Axial Turbine Cascades*. Proceedings of ASME Turbo Expo 2010: Power for Land, Sea and Air, GT2010-23808, June 14-18, 2010, Glasgow, UK
Váchová, J., Luxa, M., Príhoda, J., Šimurda, D., (2015). *Transition Model Application on Mid-Section Turbine Blade Cascade*. Proceedings of the 12th International Symposium on Experimental Computational Aerothermodynamics of Internal Flows, 13-16 July 2015, Lerici, Italy